CityU
香港城市大學
City University of Hong Kong
專業 創新 胸懷全球
Professional·Creative
For The World

CityU Scholars

Structural evolution of Na-rich spinel oxides involving anionic redox reaction for Na-ion batteries

Su, Bizhe; Liang, Hanqin; Zhao, Xiaohui; Zhang, Tao; Zhou, Yu; Yu, Denis Y.W.

Published in:
Electrochimica Acta

Published: 01/02/2023

Document Version:
Post-print, also known as Accepted Author Manuscript, Peer-reviewed or Author Final version

License:
CC BY-NC-ND

Publication record in CityU Scholars:
Go to record

Published version (DOI):
10.1016/j.electacta.2022.141746

Publication details:
Su, B., Liang, H., Zhao, X., Zhang, T., Zhou, Y., & Yu, D. Y. W. (2023). Structural evolution of Na-rich spinel oxides involving anionic redox reaction for Na-ion batteries. *Electrochimica Acta*, *440*, Article 141746. https://doi.org/10.1016/j.electacta.2022.141746

Citing this paper
Please note that where the full-text provided on CityU Scholars is the Post-print version (also known as Accepted Author Manuscript, Peer-reviewed or Author Final version), it may differ from the Final Published version. When citing, ensure that you check and use the publisher's definitive version for pagination and other details.

General rights
Copyright for the publications made accessible via the CityU Scholars portal is retained by the author(s) and/or other copyright owners and it is a condition of accessing these publications that users recognise and abide by the legal requirements associated with these rights. Users may not further distribute the material or use it for any profit-making activity or commercial gain.

Publisher permission
Permission for previously published items are in accordance with publisher's copyright policies sourced from the SHERPA RoMEO database. Links to full text versions (either Published or Post-print) are only available if corresponding publishers allow open access.

Take down policy
Contact lbscholars@cityu.edu.hk if you believe that this document breaches copyright and provide us with details. We will remove access to the work immediately and investigate your claim.

Download date: 24/04/2025

© 2022. This manuscript version is made available under the CC-BY-NC-ND 4.0 license
https://creativecommons.org/licenses/by-nc-nd/4.0/.

Structural evolution of Na-rich spinel oxides involving anionic redox reaction for Na-ion batteries

Bizhe Su [a], Hanqin Liang [b], Xiaohui Zhao [b,c], Tao Zhang [b,c], Yu Zhou[a], Denis Y. W. Yu [a,d,*]

[a] School of Energy and Environment, City University of Hong Kong, 83 Tat Chee Avenue, Hong Kong, China

[b] State Key Laboratory of High Performance Ceramics and Superfine Microstructure, Shanghai Institute of Ceramics, Chinese Academy of Sciences, Shanghai 201899, China

[c] Center of Materials Science and Optoelectronics Engineering, University of Chinese Academy of Sciences, Beijing 100049, China

[d] Center for Green Research on Energy and Environmental Materials (GREEN), National Institute for Materials Science, Tsukuba, Ibaraki 305-0044, Japan. Email: yu.denis@nims.go.jp

ABSTRACT

Two sodium-rich transition metal (TM) oxides with the same spinel structure, Na_2MoO_4 and Na_2WO_4 have been investigated as cathode materials for Na-ion batteries for the first time. Although the oxidation state of TMs in the compounds are already at its highest value of 6+, both of them can be activated by anionic redox reaction during initial charge, as revealed by X-ray photoelectron spectroscopy, to give considerable reversible capacity between 1.2 and 4.7 V. In addition, ex-situ X-ray diffractometry (XRD) shows that both cathode materials undergo insignificant structural evolution during Na extraction/insertion, suggesting that the Mo-O_4 and W-O_4 tetrahedral framework are stable even when more than 1 Na is removed from the materials. Overall, Na_2WO_4 shows larger amount of Na extraction/insertion and better cycle stability than Na_2MoO_4. This is likely due to better structural integrity and better stability of Na_2WO_4 against oxygen loss from ex-situ XRD and differential electrochemical mass spectrometry results.

Keywords: Na-ion battery; cathode materials; spinel oxides; anionic redox reactions; structural stability

1. Introduction

Electrical energy storage systems are the key component for large-scale grid technology to

store intermittent renewable energy resources, and among them, sodium-ion batteries (NIBs) are a possible candidate because of the cost-effectiveness and earth-abundance of Na.[1-3] Typical transition metal (TM) oxide cathode materials in NIBs utilize the redox reaction of the TMs in the lattice to compensate for the charge transfer during charge and discharge, but this cationic redox reaction (CRR) sets a limit to the available capacity and energy density for the corresponding NIBs. In the last decade, anionic redox reactions (ARRs) involving the charge transfer of the oxygen anions in the material structure were demonstrated to boost the capacity of Li-ion based cathode materials such as cation-disordered rocksalt TM oxides, $LiVO_3$, Li_2MnO_3 and its analogs to 250-300 mAh g^{-1} [4-7], and similar mechanism was also shown in some Na-based TM oxides in the past where the reversible capacities are more than 200 mAh g^{-1} in NIBs.[8-12]

Generally, ARR occurs in these materials because the O 2*p* orbital has higher energy level than TM 3*d* orbital and is closer to the Femi level. Since the O 2*p* orbital energy level is governed by the coordination and neighboring atoms of oxygen atoms, not all TM oxides can exhibit ARR. [13-16] So far, most ARR-involving cathode materials have TMs that are octahedrally-coordinated with oxygen. Though, irreversible cation migration (typically, the movement of transition metal ions to the empty Na sites during alkaline metal extraction) is suggested to be one main cause of voltage decay and capacity fade in these Na-based ARR-involving cathodes.[17-19] So, strengthening of the TM-O bond can be a strategy to improve the stability of the ARR-involving cathodes. Recently, our group has reported some new sodium vanadium oxides with tetrahedrally-coordinated oxygen atoms that exhibit reversible charge-discharge with ARR.[8-10] They demonstrate excellent structure stability with insignificant changes in lattice constants and cell volume during desodiation and sodiation. We attribute this to the TM-O_4 tetrahedral framework in the material that is able to maintain the structure of the materials. This opens up a new category of potential cathode materials for NIBs.

To further understand how material structure affects the stability of ARR, in this work, we studied the charge/discharge behaviors of Na_2MoO_4 and Na_2WO_4, both of which possess the same spinel structure with TM-O_4 tetrahedral arrangement with the oxidation state of TMs in their highest value of 6+. A facile solid-state reaction was used to synthesize the materials, and they were made into electrodes for electrochemical tests in NIBs. Both materials can be activated upon charging to

4.7 V with a sloping charge curve around 4.2 V which is attributed to ARR. The maximum reversible capacity is 184 and 168 mAh g^{-1} for Na_2MoO_4 and Na_2WO_4, respectively after several cycles. Ex-situ XRD results show that both materials undergo insignificant structural changes during Na^+ (de-)intercalation, which further supports that the TM-O_4 tetrahedral configurations can enable good crystal structural integrity.

2. Experimental

2.1. Material synthesis

Na_2TMO_4 (TM = Mo or Wo) was synthesized by a solid-state reaction. The precursors used were MoO_3 (Aladdin, 99.9%), WO_3 (Aladdin, 99.9%) and $NaHCO_3$ (Alfa Aesar, 99%). For Na_2MoO_4, stoichiometric ratios of MoO_3 and $NaHCO_3$ precursors were mixed by ball milling at 300 rpm for 6 hrs with ethanol (Fritsch pulverisette 7) and then the dried powder was pressed into pellets and heated to 400 °C for 12 hrs in air. Na_2WO_4 was synthesized at a higher temperature of 500 °C. After annealing, both samples were transferred after cooling immediately to a glovebox filled with argon. As the as-obtained powders are white in colour and have low electrical conductivity with Mo^{6+}/W^{6+} (d0 configuration), 65 parts of the materials was further mixed with 25 parts of acetylene black (AB) by weight in Ar with a ballmill at 400 rpm for 3 hrs.

2.2. Electrochemical characterizations

The ball-milled powders (Na_2TMO_4 with AB) were mixed with polyvinylidene fluoride (PVdF) binder with a weight ratio of 90:10 and 1-methyl-2-pyrrolidone (NMP) to make into a slurry, and the slurry was then coated onto a carbon-coated aluminum sheet (MTIXTL) to make the electrode. All procedures were conducted in the glovebox to avoid moisture in the air. The average active mass loading of the electrode is 1.2 mg cm^{-2}. Then, the electrode was cut into 16 mm diameter discs which were then pressed by a calender. They were then dried before putting into argon-filled glovebox. Coin cells (2032-type) were assembled using sodium metal as a counter electrode with 2 M $NaPF_6$ in propylene carbonate (PC) electrolyte and a glass fiber separator. The batteries were then tested with a battery tester (Neware) at 25 °C between 1.2 and 4.7 V vs. Na/Na^+. The typical charge-discharge current rate is 10 mA g^{-1}. Galvanostatic intermittent titration technique (GITT), as specified in the results and discussion part, was used to measure the diffusivity of Na in the cell during charge and discharge.

2.3. Structural characterizations

The materials structure was investigated with a laboratory powder X-ray diffraction (PANalytical X'Pert3 X-ray Diffractometer; XRD) with a Cu source (λ = 1.5406 Å). GSAS-II software was used to conduct the Rietveld refinement of XRD data.[20] The morphology of the materials was studied by scanning electron microscopy (SEM, EVOMA10, Zeiss). Surface chemical state of the electrodes was investigated with X-ray photoelectron spectroscopy (XPS) using monochromatic Al K_α X-ray source at 1486.6 eV (Thermal Scientific Corporation, Escalab 250 Energy Spectrometer), with a base pressure of 2×10^{-10} mbar. The C 1s peak at 284.4 eV was used to calibrate the spectrometer. To avoid contact with air, a dedicated transfer chamber was used to transport the samples from the glovebox to the instrument. Ar^+ beam is used for ion etching, with etching time of 1 min for the cycled electrode and the etching rate of 9 nm min^{-1} (using a standard Ta_2O_5 sample). For in-situ differential electrochemical mass spectrometry (DEMS) measurements, the mass spectrometer (MSD, Agilent, 5975C) with electron impact ion source was connected to a Swagelok-type cell, and the generated gas during charge and discharge is transported by Ar carrier gas. A fixed current of 300 μA g^{-1} was applied to the cell with active materials loading of 8.44 and 9.42 mg for the Na_2MoO_4 and Na_2WO_4 electrodes, respectively.

3. Results and discussion

Na_2MoO_4 was synthesized at 400 ℃ by a solid-state reaction and the crystal structure of the as-obtained powder was examined by XRD. The XRD profile of the sample matched that of Na_2MoO_4, with a space group of Fd-3m (lattice constants $a = b = c$ = 9.1080(2) Å) (Figure 1a).[21] In comparison to Na_2MoO_4, Na_2WO_4 was synthesized at a higher temperature of 500 ℃, and it shows the same Fd-3m structure as Na_2MoO_4, but with a larger lattice parameter of $a = b = c$ = 9.1563(6) Å because of the larger atomic size of W than Mo (Figure 1b). Figure 1c shows the crystal structure of the materials. Both Na_2MoO_4 and Na_2WO_4 possessed a classic cubic spinel structure where the arrangement of TM and alkaline metals in the structure is the reverse of that in a spinel $LiMn_2O_4$ cathode (i.e., Mo/W atoms occupy 8b sites with tetrahedral coordination, and Na atoms reside on 16c sites with regular octahedral coordination). Mo/W-O_4 were isolated from each other, while there was a 3D diffusion pathway for Na ions in the direction of (1 1 0), (0 1 1), and (1 0 1). O atoms were coordinated with 1W and 3Na in asymmetrical tetrahedrons. The 2 materials have

identical structures, as shown from the crystallographic parameters from Rietveld refinement of the materials in Table 1.

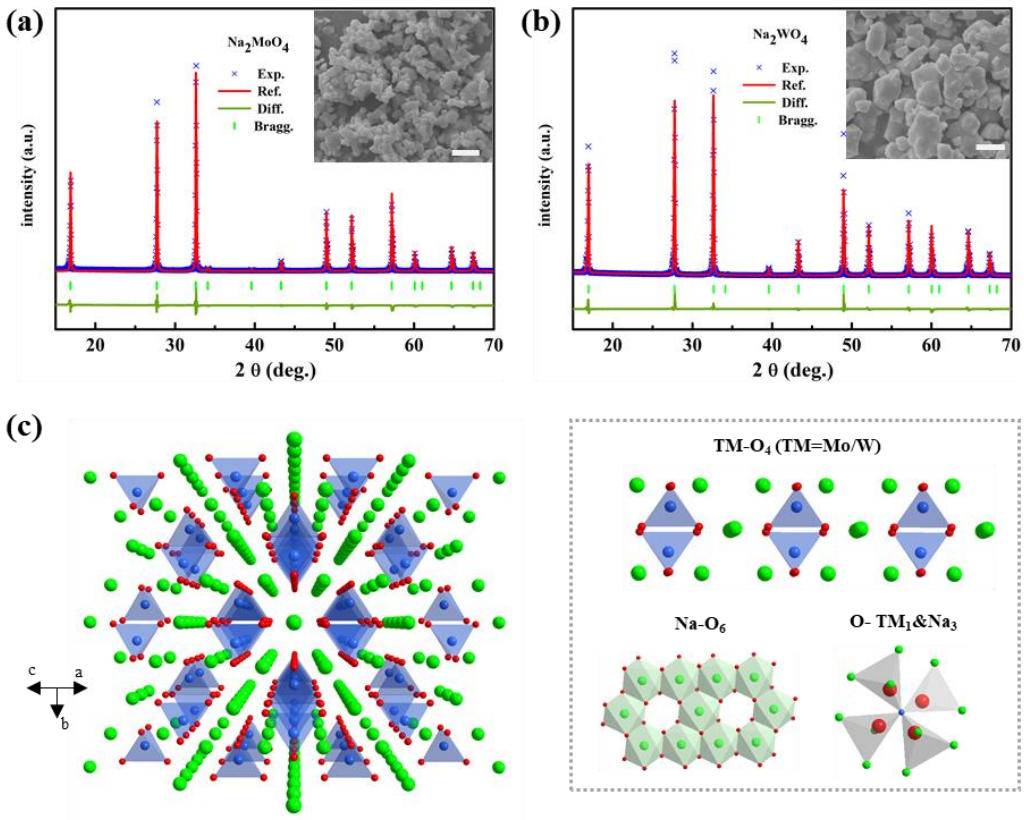

Figure 1. XRD patterns of the as-synthesized **(a)** Na_2MoO_4 and **(b)** Na_2WO_4 with inset of SEM images (scale bars is 2 μm), respectively, **(c)** The crystal structure of Na_2TMO_4 (TM = Mo or W) [Green balls – Na; red balls – O; Blue balls – Mo or W].

Table 1. Crystallographic parameters of Na_2MoO_4 and Na_2WO_4 as obtained from their XRD data with Rietveld refinement.

Formula	atom	site	x	y	z
Na_2MoO_4	Na	16c	0.0000(240)	0.0000(240)	0.0000(240)
	Mo	8b	0.3750(110)	0.3750(110)	0.3750(110)
	O	32e	0.2617(230)	0.2617(230)	0.2617(230)
Na_2WO_4	Na	16c	0.0000(90)	0.0000(90)	0.0000(90)
	W	8b	0.3750(60)	0.3750(60)	0.3750(60)

	O	32e	0.2617(40)	0.2617(40)	0.2617(40)

The particle morphology of Na_2MoO_4 and Na_2WO_4 was investigated by SEM, which the images are presented in the inset of Figure 1a and 1b. While Na_2MoO_4 showed a particle size of around 0.5–1 μm, Na_2WO_4 showed a larger particle size of around 1–2 μm due to the higher synthesis temperature. To further reduce the particle size and improve the electron conductivity of active materials, as-synthesized Na_2MoO_4 and Na_2WO_4 were ball milled with AB. The particle size of both samples was effectively reduced to sub-micron level with partial aggregation of the particles, as seen in Figure S1 and Figure S2.

Galvanostatic cycling was carried out between 1.2 V and 4.7 V versus Na/Na^+ with a typical current of 10 mA g^{-1}. In theory, Na_2MoO_4 can give a capacity of 260 mAh g^{-1} with 2 Na extraction for each formula unit. When the cell was initially discharged to 1.2 V to examine the capacity from reduction of TM alone, it reveals an insignificant discharge capacity of 9 mAh g^{-1} (Figure S3). This suggest that the material cannot accommodate extra Na beyond Na_2MoO_4 in the lattice when the voltage is lowered to 1.2 V from the reduction of Mo from 6+ to 5+. Interestingly, when Na_2MoO_4 is initial charged to 4.7 V, the material can be activated with a sloping voltage profile with a large initial charge capacity of 145 mAh g^{-1}, which corresponds to the removal of 1.12 Na from the structure (Figure 2a). Since Mo is in its highest oxidation state (i.e., a valence state of 6+) with a d0 configuration in Na_2MoO_4, it is unlikely that Mo can be further oxidized during the charging process. This would suggest that the observed electrochemical activity originates from the oxidation reaction of O^{2-} (ARR). Unlike the pristine materials, the charged material with $Na_{2-x}MoO_4$ can be discharged to 1.2 V, where about 0.93 Na (corresponding to a capacity of 121 mAh g^{-1}) can be re-inserted back into the lattice with an initial Coulombic efficiency (CE) of 83.4%. This indicate that the electrochemical activity of Na_2MoO_4 is reversible after an activation process to 4.7 V. There may be some degree of electrolyte decomposition and side reactions between the electrolyte and the surface of the active materials when charged to a high cut-off voltage, but the charge capacity is not mostly from electrolyte decomposition, as first of all, the pure Al current collector gives negligible capacity when charged to 4.7 V, as observed in our previous work. [9] In addition, cells with electrolyte decomposition typically cannot be discharged, which is not the case here. During

the second charge, the voltage profile is different from the first charge, which is a common feature for ARR-involving cathode materials as the charge transfer mechanism is changed during the initial cycle. Upon further cycling, the specific capacity increases and voltage hysteresis decreases. This indicates that the material undergoes further activation during cycling, as evidence from the small plateau above 4.2 V during charging, probably because the material has low electrical conductivity and the kinetics of ARR is slow.[22, 23] The highest discharge capacity that is obtained from Na_2MoO_4 is 184 mAh g^{-1} during the sixth cycle, corresponding to 1.45 Na inserted into the structure. With prolonged cycling, the capacity of Na_2MoO_4 gradually decreases, possibly due to side reactions such as electrolyte decomposition since the upper cutoff voltage is 4.7 V (Figure S4). In addition, as shown later, there are some amount of oxygen release from the material at high voltage.

For Na_2WO_4, its theoretical capacity is 182 mAh g^{-1} assuming 2 Na removal and insertion. Similar to Na_2MoO_4, Na_2WO_4 only gives a negligible capacity of 6 mAh g^{-1} if the electrode is initial discharged to 1.2 V (Figure S5), indicating that W in Na_2WO_4 cannot be reduced down to 1.2 V. However, when we charge the material to 4.7 V, the initial capacity is 112 mAh g^{-1} (corresponding to 1.22 Na extraction), with a reversible discharge capacity of 98 mAh g^{-1} to 1.2 V and an initial CE ~87.5%, as shown in Figure 2b. Similar to Na_2MoO_4, with further activation, the reversible capacity increases after initial cycles to 168 mAh g^{-1} during the sixth cycle, corresponding to 1.85 Na insertion into the structure. Na_2WO_4 shows a stable capacity of about 160 mAh g^{-1} for 30 cycles (Figure S4).

Na_2MoO_4 and Na_2WO_4 showed similar voltage profiles upon cycling, suggesting that they undergo a similar electrochemical mechanism during charge and discharge. Even though the initial specific capacity of Na_2WO_4 is lower than that of Na_2MoO_4, more Na can be extracted/inserted reversibly in Na_2WO_4 per unit formula (per mole) as it has a higher molecular weight. When the charge/discharge curves are compared, Na_2WO_4 shows higher number of Na extracted and inserted, but also a larger voltage hysteresis (a maximum of around 1.98 V for Na_2WO_4 and 1.72 V for Na_2MoO_4) (Figure S6). This is possibly due to the higher ionicity of W^{6+} that resulted in stronger interactions with the coordinated oxygen anions as compared to that of Mo^{6+}, i.e., the bond dissociation energies of Mo-O and W-O are 607(34) and 653(25) kJ mol^{-1}, respectively.[24]

Even though initial capacity of Na_2WO_4 is lower than that of Na_2MoO_4, Na_2WO_4 shows better cycle performance than Na_2MoO_4, as shown in Figure S4. Note that the initial CE for both electrodes is only around 88%, which is further decreased to above 83% after 10 cycles. This suggests that there were other side reactions, such as electrolyte decomposition, taking place during charge/discharge which need to be further studied and suppressed in the future.

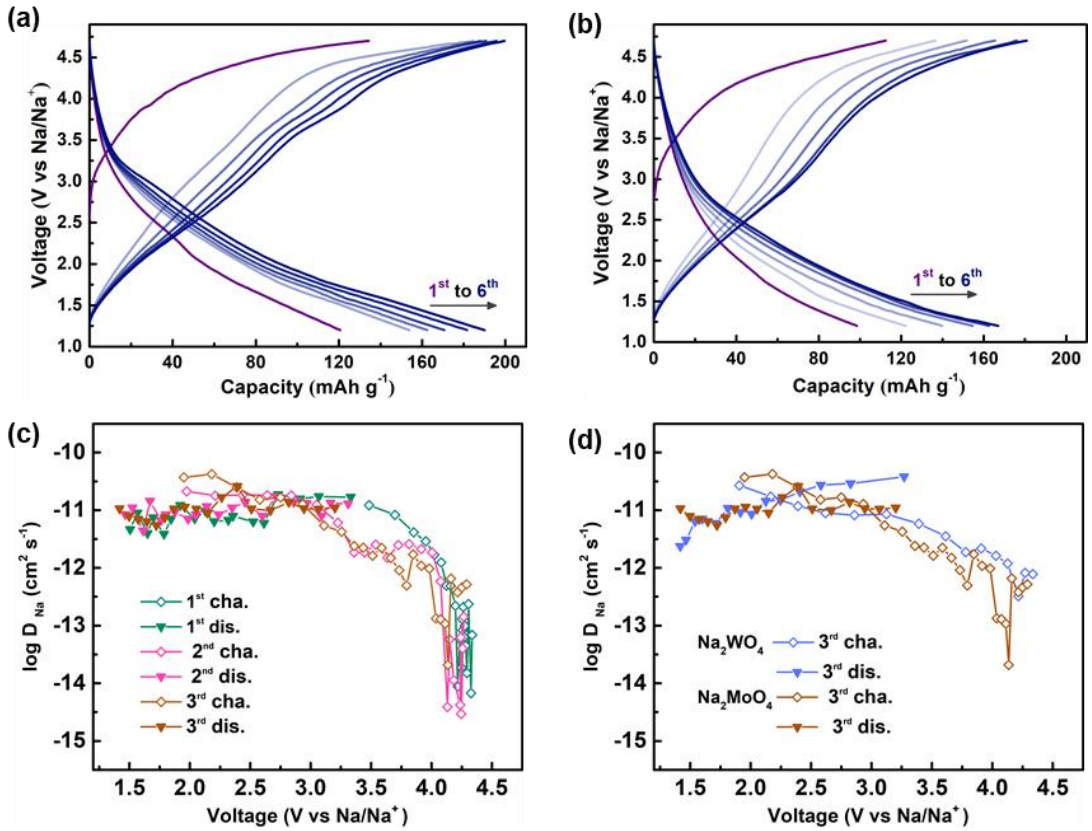

Figure 2. Galvanostatic charge/discharge curves of **(a)** Na_2MoO_4 and **(b)** Na_2WO_4 between 1.2 V and 4.7 V with 10 mA g^{-1} in the initial cycles. **(c)** The Na^+ diffusion coefficients of Na_2MoO_4 calculated from GITT in the range of 1.2-4.7 V during the initial three cycles **(d)** Comparison of Na^+ chemical diffusion coefficients of Na_2MoO_4 and Na_2WO_4 calculated from GITT in the range of 1.2-4.7 V during the third cycle.

We further analyzed the charge-discharge mechanism using Na_2MoO_4 as a sample material by *ex-situ* XPS during the first electrochemical cycle between 1.2 and 4.7 V at different states of charge. Figure 3 shows the core XPS spectra for Mo and O. For the Mo 3*d*3/2 and 3*d*5/2 profiles, Ar ion etching was not conducted because etching can reduces the valence state of the transition metal. On the other hand, Ar ion etching is conducted for the O 1*s* profiles to remove the surface deposits to

obtain the bulk information.[7, 8] The Mo 3*d*3/2 and 3*d*5/2 spectrum of the pristine Na_2MoO_4 electrode shows peaks at 236.2 eV and 233.1 eV, respectively, corresponding to a Mo oxidation state of 6+.[25-27] When the electrode was charged to 4.7 V, there is no change in the XPS profile and peak position of Mo. This suggests that Mo remains 6+ after charging. In comparison, new peaks attributed to Mo^{4+} appears at 234.1 eV and 231.1 eV after discharging to 1.2 V [28], and the peak area of Mo^{6+} decreases accordingly.

As for the O 2*p* spectra, a peak attributed to O^{2-} can be seen for the pristine Na_2MoO_4 material at 531.0 eV.[29] Charging the electrode to 4.7 V results in the formation of a new peak at 531.7 eV. This indicates the presence of peroxo-species in the material, which contributes to the charge transfer during initial charge.[30-32] The intensity of this peroxo-species peak is reduced after the cell is discharged to 1.2 V, indicating that the oxygen redox reaction is partial reversible. Overall, the results suggest that Na_2MoO_4 is activated by oxygen reaction with ARR during initial charge while Mo remaining 6+. During discharge, both CRR of Mo and ARR of O contribute to the observed reversible capacity, which continues during subsequent cycles. Similar charge-discharge mechanism can be expected for Na_2WO_4 as well because of the similar charge-discharge curves and electrochemical behaviors as Na_2MoO_4. For ARR-involving cathode materials, peroxide species were reported with oxygen oxidation during initial charge. Seo et al. suggested that the strength of the M-O bonds in the materials influences the formation of peroxide species. In particular, transition metals with no *d* shells (in this case Mo^{6+} and W^{6+}) provide a weaker and less directional M-O bonds, which facilitate O-O bonds formation.[15]

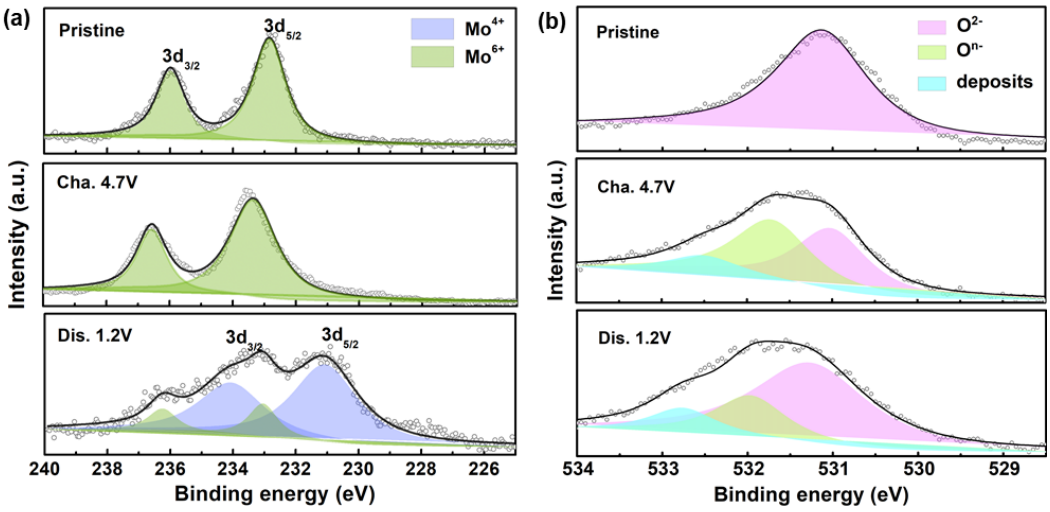

Figure 3. (a) *Ex-situ* Mo 3*d*3/2 and 3*d*5/2 XPS core spectra and (b) O 1*s* profiles obtained from Na_2MoO_4 electrodes at different state-of-charge during the first cycle.

To evaluate the Na^+ diffusion coefficient of the cathode materials, GITT was performed during the initial three cycles on cells between 1.2 -4.7 V at 10 mA g^{-1}. The GITT profiles of Na_2MoO_4 and Na_2WO_4 are showed in Figure 2c, 2d, S7 and S8, respectively, which reveal large polarization across the entire voltage range, possibly due to the low kinetics of ARRs. The Na^+ diffusion coefficient is calculated by Eq. 1:

$$D = \frac{4}{\pi\tau}\left[\frac{m_B V_M}{M_B A}\right]^2 \left[\frac{\Delta E_S}{\Delta E_t}\right]^2 \qquad (1)$$

Where A is the area of the electrode (= 2.01 cm^2), m_B is the weight of the active materials (0.00252 g and 0.00248 g for Mo- and W-based electrodes, respectively in the case) and τ is the duration of the current pulse (= 3600 s). M_B and V_M are molecular weight and molar volume of the cathode materials, respectively. During the current pulse, the steady-state voltage change is ΔE_S while after the pulse, the voltage change is ΔE_t. The diffusivity calculated for the initial three cycles of Na_2MoO_4 is about 10^{-11} cm^2 s^{-1} during discharge (sodiation), while during charging, diffusivity gradually decreases to about 10^{-13} cm^2 s^{-1} as the voltage is increased (Figure 2c). For comparison, the trend of the Na diffusivity of Na_2WO_4 is similar to that of Na_2MoO_4, as shown in Figure 2d.

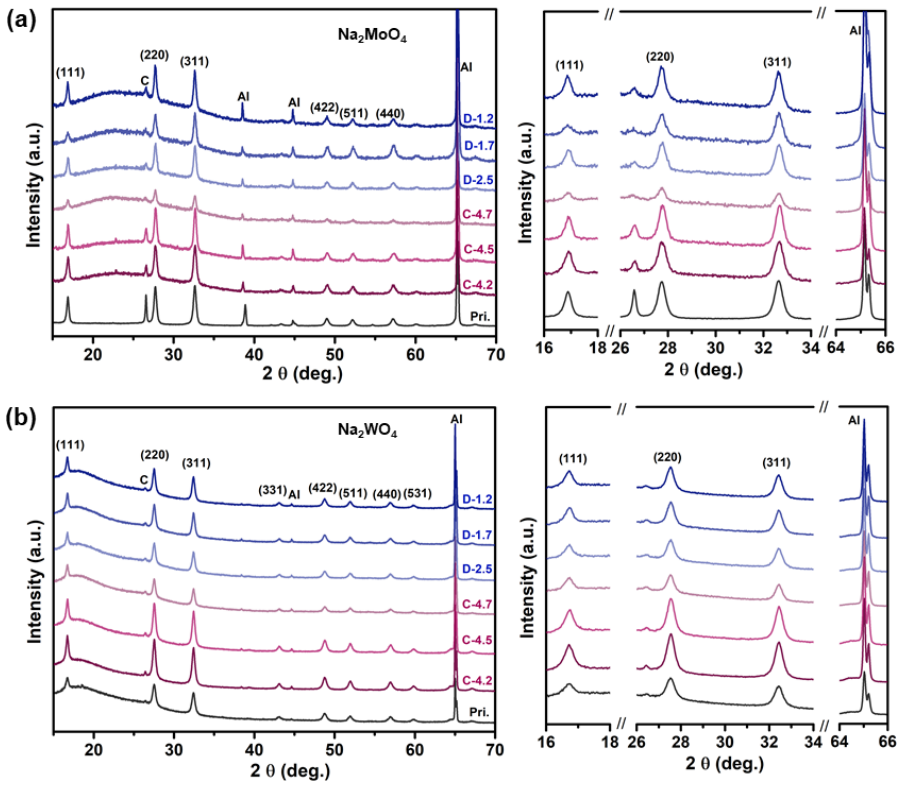

Figure 4. Ex-situ XRD profiles of **(a)** Na_2MoO_4 and **(b)** Na_2WO_4 electrodes at different charged states between 1.2 V and 4.7 V during the 1st cycle. [The number in C-# corresponds to the cutoff charge voltage; D-# refers to an electrode initially charged to 4.7 V, and then discharged to targeted discharge voltage]

Ex-situ XRD tests were used to study the structural variation of Na_2MoO_4 and Na_2WO_4 electrodes at different states of charge during Na^+ extraction/insertion, and the corresponding XRD profiles are shown in Figure 4. Upon Na-ion extraction, no new peak is formed and there is also no apparent peak shift for both materials. These suggest that the structure of the material is not changed, and no new phases are formed during de-sodiation. Overall, XRD peak intensities for both materials decrease when they are charged to 4.7 V, which may be due to a reduced atomic scattering factor from the removal of more than half of the sodium from the structure, as the peak intensities recover upon discharge. The change in the *a* lattice parameters of both Na_2MoO_4 and Na_2WO_4 electrodes is negligible, only about 0.005% and 0.007%, respectively after charging during the first cycle to 4.7 V, suggesting that the TM-O_4 framework is stable against Na extraction.

Even upon cycling, the structure of the materials does not change. After 20 cycles, both materials show XRD peaks corresponding to the original Na_2MoO_4 and Na_2WO_4 structure (Figure

S9), indicating the structure is invariant upon charge and discharge. For Na_2WO_4, sharp peaks can still be clearly seen after 20 cycles (Figure S9b), indicating stable structure and cycle performance. In comparison, Na_2MoO_4 electrode shows reduced peak intensities after 20 cycles. This suggests some degree of structural degradation of Na_2MoO_4, which is consistent with the capacity decay as observed during cycling (Figure S4).

To further study the stability of Na_2MoO_4 and Na_2WO_4 during charge and discharge, the gas formed from the electrodes during the initial charge process was studied by DEMS (Figure 5). Our results indicate that near the end of the charged state, there is a small amount of oxygen gas released for Na_2MoO_4 electrode above 4.5 V. In comparison, no oxygen gas can be detected from the Na_2WO_4 electrode during charging. The better stability of Na_2WO_4 may be attributed to the higher bond dissociation energy of W-O than Mo-O. [24] Though, the kinetics of oxygen release may be another factor which needs further characterizations in the future. [35] Meanwhile, the CO_2 gas release is detected for both electrodes probably from side reaction between electrode and electrolyte (see Figure S10). DEMS results further elaborate the change in XRD and cycle performance, suggesting that there is some degradation of Na_2MoO_4 with cycling, whereas Na_2WO_4 is more stable within the tested voltage range. Further work, such as inductively-couple plasma spectroscopy of the electrolyte to study the amount of TM dissolution from the active material, may give more insights into the degradation mechanism of the materials.

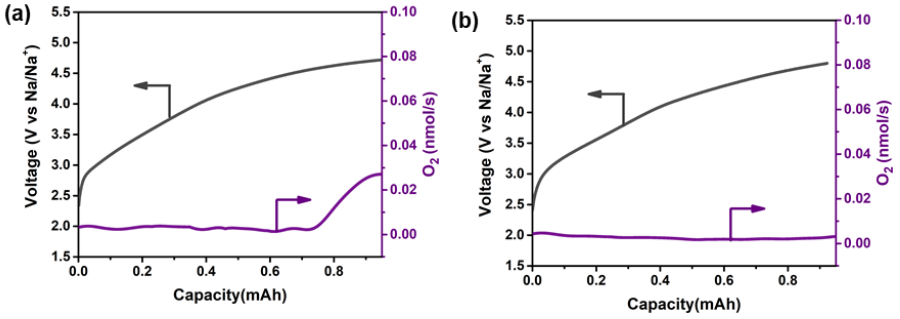

Figure 5. Oxygen gas evolution in **(a)** Na_2MoO_4 and **(b)** Na_2WO_4 electrodes as determined by in-situ DEMS during the initial charge process. Voltage profiles of the electrodes are included.

4. Conclusions

In this work, for the first time, two sodium-rich spinel oxides, Na_2MoO_4 and Na_2WO_4, with TM-O_4 tetrahedral configuration were studied as cathode materials for NIBs. The results

demonstrated that although TMs (Mo or W) are in the highest oxidation state in the pristine compounds, the materials can still be charged with a large capacity until 4.7 V, which is attributed to ARR in the materials. After activation, the materials undergo reversible charge and discharge with redox reactions of both the TM and O. Ex-situ XRD tests reveal that the materials are near zero-strain during de-sodiation/sodiation with negligible change in lattice parameters. Even after 20 cycles, the original spinel structure can still be observed in the material, which suggests that the TM-O_4 tetrahedral framework is robust. Between the two materials, Na_2WO_4 cathode shows a better stability against oxygen loss and structural degradation than Na_2MoO_4. This work provides insights on the stability of ARR-involving cathode materials and can propel the search for other novel cathode materials for NIB in the future.

Acknowledgements

This work was supported by the Research Grants Council (CityU 11304518) of the Hong Kong Special Administrative Region, China.

References:

[1] S. Wang, C. Sun, N. Wang, Q. Zhang, Ni-and/or Mn-based layered transition metal oxides as cathode materials for sodium ion batteries: status, challenges and countermeasures, J. Mater. Chem. A, 7 (2019) 10138-10158.

[2] M. Chen, Q. Liu, S.W. Wang, E. Wang, X. Guo, S.L. Chou, High-abundance and low-cost metal-based cathode materials for sodium-ion batteries: problems, progress, and key technologies, Adv. Energy Mater., 9 (2019) 1803609.

[3] W.-J. Li, C. Han, W. Wang, F. Gebert, S.-L. Chou, H.-K. Liu, X. Zhang, S.-X. Dou, Commercial Prospects of Existing Cathode Materials for Sodium Ion Storage, Adv. Energy Mater., 7 (2017) 1700274.

[4] N. Yabuuchi, K. Yoshii, S.T. Myung, I. Nakai, S. Komaba, Detailed studies of a high-capacity electrode material for rechargeable batteries, Li_2MnO_3-$LiCo_{(1/3)}Ni_{(1/3)}Mn_{(1/3)}O_2$, J. Am. Chem. Soc, 133 (2011) 4404-4419.

[5] A.D. Robertson, P.G. Bruce, Mechanism of electrochemical activity in Li_2MnO_3, Chem. Mater., 15 (2003) 1984-1992.

[6] H. Yu, H. Zhou, High-Energy Cathode Materials (Li_2MnO_3-$LiMO_2$) for Lithium-Ion Batteries, J Phys. Chem. Lett., 4 (2013) 1268-1280.

[7] B. Su, S. Wu, H. Liang, Q. Gu, H. Wang, W. Zhou, X. Zhao, T. Zhang, P.H.L. Sit, W. Zhang, D.Y.W. Yu, Boosting capacity and operating voltage of $LiVO_3$ as cathode for lithium-ion batteries by activating oxygen reaction in the lattice, J. Power Sources, 517 (2022) 230728.

[8] B. Su, S. Wu, H. Liang, W. Zhou, J. Liu, D. Goonetilleke, N. Sharma, P.H.L. Sit, W. Zhang, D.Y.W. Yu, High-Performance $NaVO_3$ with Mixed Cationic and Anionic Redox Reactions for Na-Ion Battery Applications, Chem. Mater., 32 (2020) 8836-8844.

[9] B. Su, H. Liang, J. Liu, J. Wu, N. Sharma, Q. Gu, B. Johannessen, D.Y.W. Yu, Novel structurally-stable Na-rich $Na_4V_2O_7$ cathode material with high reversible capacity by utilization of anion redox activity, Chem. Commun., 56 (2020) 8245-8248.

[10] J. Zhang, B. Su, A. Kitajou, M. Fujita, Y. Cui, M. Oda, W. Zhou, P.H.L. Sit, D.Y.W. Yu, Activating abnormal capacity in stoichiometric $NaVO_3$ as cathode material for sodium-ion battery, J. Power Sources, 400 (2018) 377-382.

[11] K. Sato, M. Nakayama, A.M. Glushenkov, T. Mukai, Y. Hashimoto, K. Yamanaka, M. Yoshimura, T. Ohta, N. Yabuuchi, Na-Excess Cation-Disordered Rocksalt Oxide: $Na_{1.3}Nb_{0.3}Mn_{0.4}O_2$, Chem. Mater., 29 (2017) 5043-5047.

[12] Q. Wang, W. Yang, F. Kang, B. Li, $Na_2Mn^{3+}{}_{0.3}Mn^{4+}{}_{2.7}O_{6.85}$: A cathode with simultaneous cationic and anionic redox in Na-ion battery, Energy Storage Mater., 14 (2018) 361-366.

[13] G. Assat, J.-M. Tarascon, Fundamental understanding and practical challenges of anionic redox activity in Li-ion batteries, Nat. Energy, 3 (2018) 373-386.

[14] N. Yabuuchi, Solid-state Redox Reaction of Oxide Ions for Rechargeable Batteries, Chem. Lett., 46 (2017) 412-422.

[15] D.H. Seo, J. Lee, A. Urban, R. Malik, S. Kang, G. Ceder, The structural and chemical origin of the oxygen redox activity in layered and cation-disordered Li-excess cathode materials, Nat. Chem., 8 (2016) 692-697.

[16] J. Hong, W.E. Gent, P. Xiao, K. Lim, D.H. Seo, J. Wu, P.M. Csernica, C.J. Takacs, D. Nordlund, C.J. Sun, K.H. Stone, D. Passarello, W. Yang, D. Prendergast, G. Ceder, M.F. Toney, W.C. Chueh, Metal-oxygen decoordination stabilizes anion redox in Li-rich oxides, Nat. Mater., 18 (2019) 256-265.

[17] R.A. House, U. Maitra, M.A. Perez-Osorio, J.G. Lozano, L. Jin, J.W. Somerville, L.C. Duda, A. Nag, A. Walters, K.J. Zhou, M.R. Roberts, P.G. Bruce, Superstructure control of first-cycle voltage hysteresis in oxygen-redox cathodes, Nature, 577 (2020) 502-508.

[18] R.A. House, U. Maitra, L. Jin, J.G. Lozano, J.W. Somerville, N.H. Rees, A.J. Naylor, L.C. Duda, F. Massel, A.V. Chadwick, S. Ramos, D.M. Pickup, D.E. McNally, X. Lu, T. Schmitt, M.R. Roberts, P.G. Bruce, What Triggers Oxygen Loss in Oxygen Redox Cathode Materials?, Chem. Mater., 31 (2019) 3293-3300.

[19] E. Talaie, S.Y. Kim, N. Chen, L.F. Nazar, Structural Evolution and Redox Processes Involved in the Electrochemical Cycling of P2–$Na_{0.67}[Mn_{0.66}Fe_{0.20}Cu_{0.14}]O_2$, Chem. Mater., 29 (2017) 6684-6697.

[20] B.H. Toby, R.B. Von Dreele, GSAS-II: the genesis of a modern open-source all purpose crystallography software package, J. Appl. Crystallogr., 46 (2013) 544-549.

[21] A.D. Fortes, Crystal structures of spinel-type Na_2MoO_4 and Na_2WO_4 revisited using neutron powder diffraction, Acta Crystallogr. E: Crystallogr. Commun., 71 (2015) 592-596.

[22] A. Konarov, J.H. Jo, J.U. Choi, Z. Bakenov, H. Yashiro, J. Kim, S.-T. Myung, Exceptionally highly stable cycling performance and facile oxygen-redox of manganese-based cathode materials for rechargeable sodium batteries, Nano Energy, 59 (2019) 197-206.

[23] J. Wu, Z. Zhuo, X. Rong, K. Dai, Z. Lebens-Higgins, S. Sallis, F. Pan, L.F. Piper, G. Liu, Z. Hussain, Dissociate lattice oxygen redox reactions from capacity and voltage drops of battery electrodes, Sci. Adv., 6 (2020) eaaw3871.

[24] J. A. Dean, Lange's Handbook of Chemistry, Fifteenth Edition, McGraw-Hill, Inc. (1999) Table 4.11.

[25] Y. Xu, M. Zhou, X. Wang, C. Wang, L. Liang, F. Grote, M. Wu, Y. Mi, Y. Lei, Enhancement of Sodium Ion Battery Performance Enabled by Oxygen Vacancies, Angew. Chem. Int. Ed. Engl., 54 (2015) 8768-8771.

[26] S. Xu, H. Ma, S. Dai, Z. Jiang, Study on optical and electrical switching properties and phase transition mechanism of Mo^{6+}-doped vanadium dioxide thin films, J. Mater. Sci., 39 (2004) 489-493.

[27] Y. Zang, C.-X. Ding, X.-C. Wang, Z.-Y. Wen, C.-H. Chen, Molybdenum-doped lithium-rich layered-structured cathode material $Li_{1.2}Ni_{0.2}Mn_{0.6}O_2$ with high specific capacity and improved rate performance, Electrochim. Acta, 168 (2015) 234-239.

[28] J.-G. Choi, L. Thompson, XPS study of as-prepared and reduced molybdenum oxides, Appl. Surf.

Sci., 93 (1996) 143-149.

[29] J. Fan, G. Li, D. Luo, C. Fu, Q. Li, J. Zheng, L. Li, Hydrothermal-Assisted Synthesis of Li-Rich Layered Oxide Microspheres with High Capacity and Superior Rate-capability as a Cathode for Lithium-ion Batteries, Electrochim. Acta, 173 (2015) 7-16.

[30] X. Zhang, Y. Qiao, S. Guo, K. Jiang, S. Xu, H. Xu, P. Wang, P. He, H. Zhou, Manganese-Based Na-Rich Materials Boost Anionic Redox in High-Performance Layered Cathodes for Sodium-Ion Batteries, Adv. Mater., 31 (2019) e1807770.

[31] Y. Wang, L. Wang, H. Zhu, J. Chu, Y. Fang, L. Wu, L. Huang, Y. Ren, C.J. Sun, Q. Liu, X. Ai, H. Yang, Y. Cao, Ultralow-Strain Zn-Substituted Layered Oxide Cathode with Suppressed P2–O2 Transition for Stable Sodium Ion Storage, Adv. Funct. Mater., 30 (2020) 1910327.

[32] Q. Wang, S. Mariyappan, G. Rousse, A.V. Morozov, B. Porcheron, R. Dedryvere, J. Wu, W. Yang, L. Zhang, M. Chakir, M. Avdeev, M. Deschamps, Y.S. Yu, J. Cabana, M.L. Doublet, A.M. Abakumov, J.M. Tarascon, Unlocking anionic redox activity in O3-type sodium 3d layered oxides via Li substitution, Nat. Mater., 20 (2021) 353-361.

[33] K. Luo, M.R. Roberts, R. Hao, N. Guerrini, D.M. Pickup, Y.S. Liu, K. Edstrom, J. Guo, A.V. Chadwick, L.C. Duda, P.G. Bruce, Charge-compensation in 3d-transition-metal-oxide intercalation cathodes through the generation of localized electron holes on oxygen, Nat. Chem., 8 (2016) 684-691.

[34] M. Saubanère, E. McCalla, J.M. Tarascon, M.L. Doublet, The intriguing question of anionic redox in high-energy density cathodes for Li-ion batteries, Energy Environ. Sci., 9 (2016) 984-991.

[35] X. Yu, Releasing oxygen from the bulk, Nat. Energy, 6 (2021) 572-573.